Supplementary Material

S1. Microscope

The LEDs were characterized using the microscope shown in Fig. S1. The emission was collected using a 0.95NA objective and was routed either into an InGaAs camera for wide-field imaging or into a single-mode fiber (SMF) by flipping a mirror (M). Through the SMFs, the emission was delivered into a photodiode or a spectrometer. A 1100 nm LED was used as the illumination to take reflection micrographs.

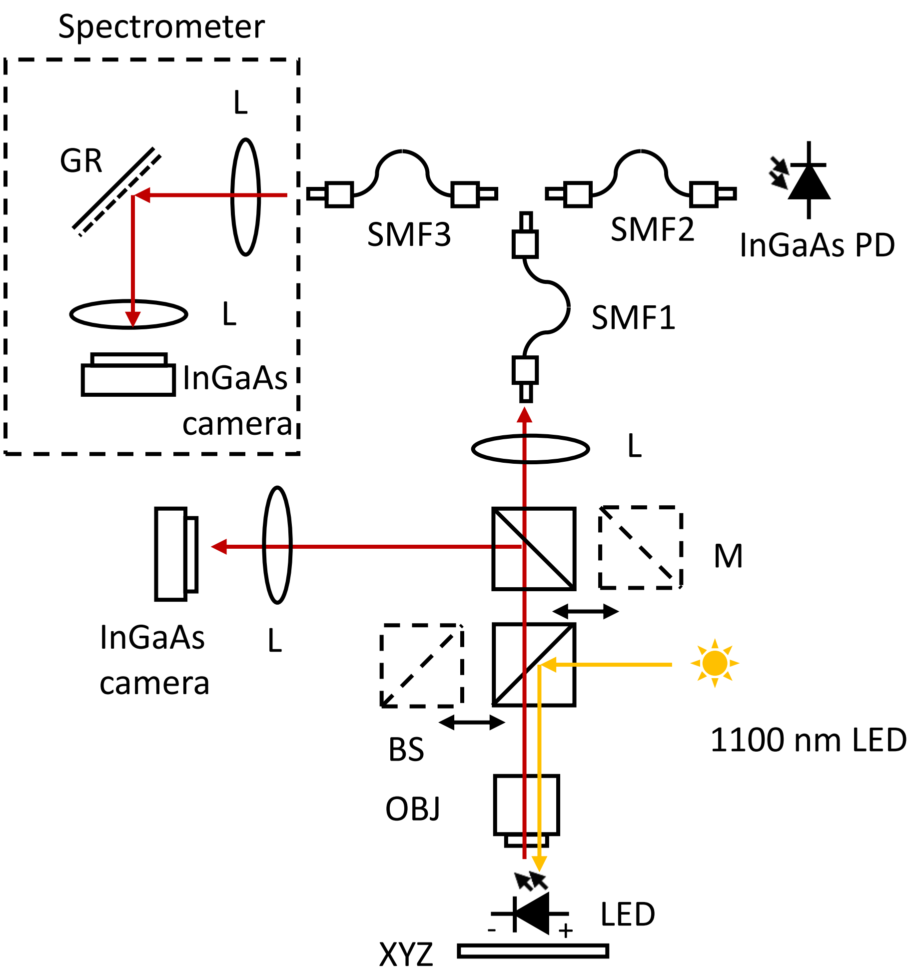

Figure S1. Schematic of the microscope used in this study. SMF: single-mode fiber; InGaAs PD: InGaAs photodiode; GR: grating; L: lens; M: mirror; BS: broadband beam splitter; OBJ: 0.95NA objective; XYZ: xyz piezo stage. The mirror and the beam splitter can be inserted and removed from the optical path.

S2. Point-spread-function correction

The Point-spread-function (PSF) of the microscope was calibrated using a reflective target sample with sharp edges. The edges were fit into erf functions which were used to extract the full-width-half-maximum (FWHM) of the PSF. The illumination was from a 1100 nm LED to minimize the wavelength dependence of the PSF.

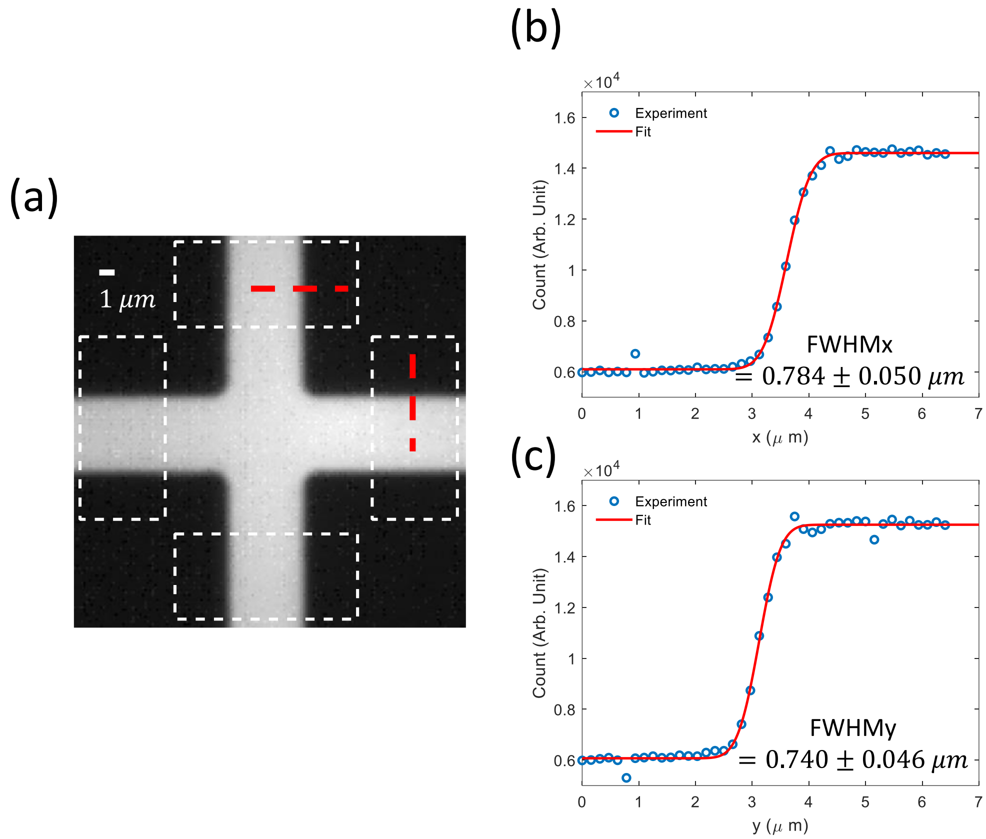

Figure S2. (a) A micrograph of the reflective sample. The red dashed lines correspond to the fit results in (b) and (c). The errors are the standard deviations from the edges in the white dashed boxes.

S3. Transmission and InGaAs camera correction

The transmission of the microscope was calibrated by back-propagating amplified spontaneous emission (ASE) of a semiconductor optical amplifier (SOA) from SMF1. An iris was used to match the beam size of the collimated ASE with the back aperture of the objective. The ASE spectrum is centered around 1130 nm, which is close to our emitter.

We measured the power of the ASE after the flipping mirror and after the objective. The transmission is approximately 50.1% and 56.2% when the ASE is x-polarized and y-polarized, respectively. The polarization dependence is due to the two dichroic mirrors (not shown in Fig. S1) between the objective and the flipping mirror. We used 53% as the transmission to correct the emission power measured directly by the camera and the photodiode. Note that this correction does not compensate for the power loss from the fiber coupling.

According to the factory test, the full well capacity and the ADC of our InGaAs camera are 1282000 and 16-bit, respectively, which corresponds to sensitivity of approximately 19.56 photo-electrons/count. The quantum efficiency is approximately 75% around 1100 nm. We thus can translate the camera count to the photon number by 26.1 photons/count.

S4. Gaussian fit and deconvolution

The images of the emission patterns were fit into two Gaussian functions with a constant.

$$I(x,y) = A_1 \exp\left(-\frac{\left(x - x_{0,1}\right)^2}{2\sigma_{x,1}^2} - \frac{\left(y - y_{0,1}\right)^2}{2\sigma_{y,1}^2} \right) + A_2 \exp\left(-\frac{\left(x - x_{0,2}\right)^2}{2\sigma_{x,1}^2} - \frac{\left(y - y_{0,2}\right)^2}{2\sigma_{y,1}^2} \right) + C \qquad \text{(Eq. S1)}$$

where the first Gaussian denotes the n+/n spot and the other two terms denote the background. The fit area is $20 \times 20\ \mu\mathrm{m}^2$. In the main text, we used the integral of the first Gaussian together with the transmission and camera sensitivity to estimate the n+/n emission power in Fig. 2(e).

In Fig. S3 the FWHM of the n+/n spot versus the bias current is presented. The curves labeled as fit are the Gaussian fit results from Eq. S1, which are from convolution of the n+/n emission pattern and the PSF of the microscope. We assume both the emission pattern and the PSF are Gaussian-shaped and the deconvolved FWHM can be thus computed as

$$FWHM_{x/y,decon} = \sqrt{FHHM_{x/y,fit}^2 - FHHM_{x/y,PSF}^2} \qquad \text{(Eq. S2)}$$

The deconvolved FWHMs are used to estimate the emission area in Fig. 2 (h).

From 1 mA to 6 mA the deconvolved FWHM decreases monotonically from $0.82\ \mu m$ to $0.33\ \mu m$ in x, while the FWHM in y remains approximately $0.5\ \mu m$ below 4 mA and decreases to 0.35 μm at 6 mA. This trend is consistent with the carrier transport process in which the holes are confined by the electrical field from the Si filament and the localization becomes stronger with the increasing bias. The deviation of the FWHM in y from the trend under low bias is probably because the holes are confined by the STI in ±y instead of the field when the current is below 4 mA. While the STI does not exist in −x, the emission pattern is more extended in x when the bias is low. (Fig. 1 (c))

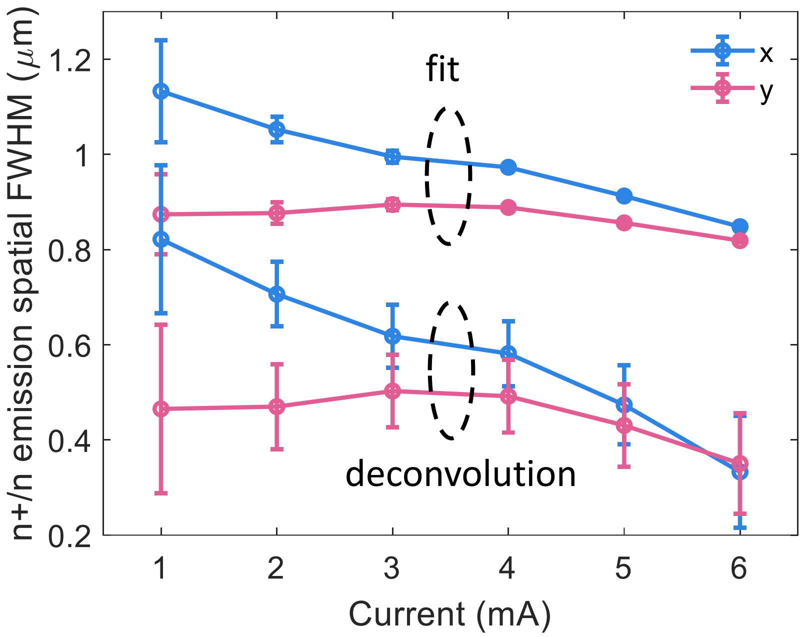

Figure S3. The FWHMs of the n+/n spot versus the bias current.

S5. Benchmark

The emission area of our LED is the smallest among the reported Si LEDS. The intensity is comparable with other state-of-the-art Si LEDs with much larger emission areas.

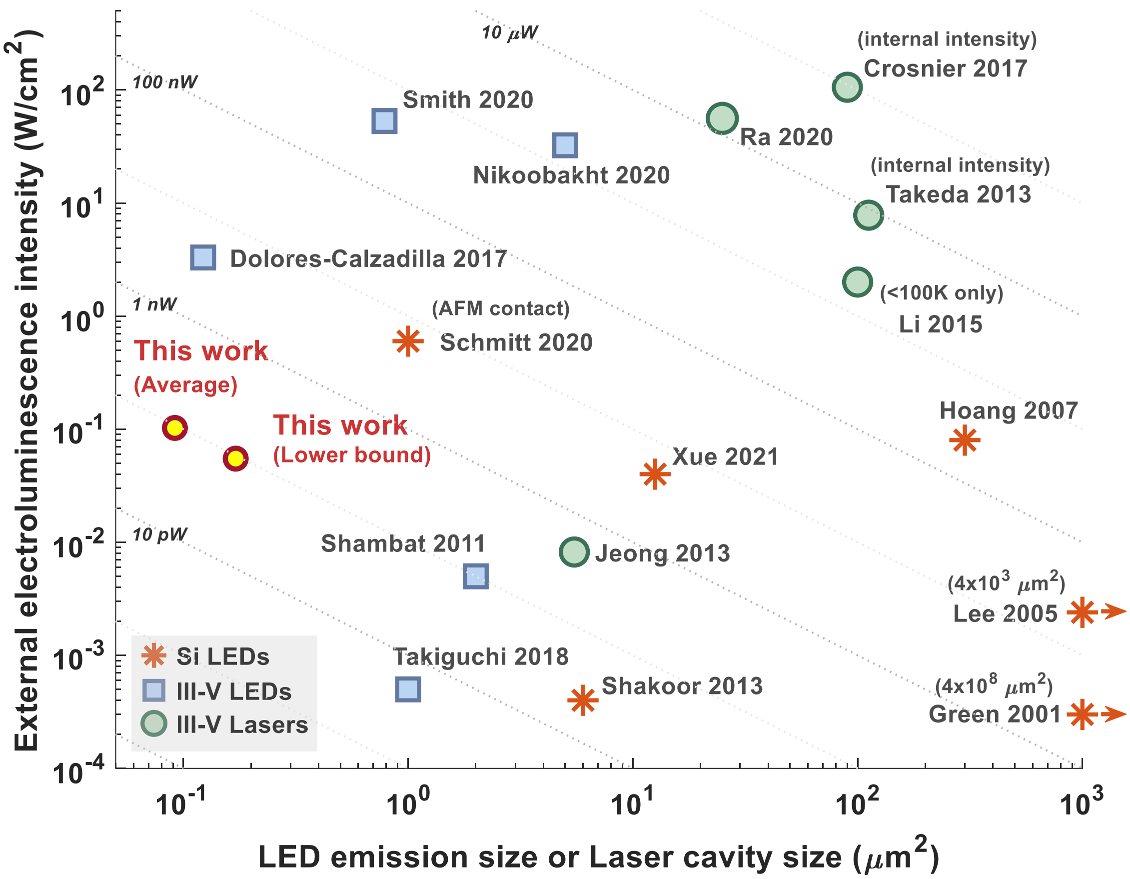

Figure S4. Benchmark of our LED compared with other related work.

Reference:

Green, et al. *Nature* 412.6849 (2001): 805-808.

Lee, et al. *Solid-state electronics* 49.7 (2005): 1172-1178.

Shakoor, et al. *Laser & Photonics Reviews* 7.1 (2013): 114-121.

Xue, et al. *IEEE Transactions on Electron Devices* 68.8 (2021): 3870-3875.

Shambat, et al. *Nature communications* 2.1 (2011): 1-6.

Dolores-Calzadilla, et al. *Nature Communications* 8.1 (2017): 1-8.

Takiguchi, et al. *Applied Physics Letters* 112.25 (2018): 251106.

Nikoobakht, et al. *Science advances* 6.33 (2020): eaba4346.

Smith, et al. *Applied Physics Letters* 116.7 (2020): 071102.

Jeong, et al. *Nature communications* 4.1 (2013): 1-6.

Takeda, et al. *Nature Photonics* 7.7 (2013): 569-575.

Li, et al. *Nature nanotechnology* 10.2 (2015): 140-144.

Crosnier, et al. *Nature Photonics* 11.5 (2017): 297-300.

Ra, et al. *Science advances* 6.1 (2020): eaav7523.

Schimitt, et al. *APL Materials*. 8, (2020): 061110

Hoang, et al. *IEEE Electron Device Letters*. 28.5 (2007): 383-385

S6. Variance and robustness

In Fig. S5, SMF-coupled power and forward bias voltage versus current of five LEDs on different chips are presented. These curves were measured right after gate oxide breakdown. In Fig. S5 (a), three curves almost overlap while the other two are approximately $\pm 20\%$ deviated. The variance is probably due to the spatial randomness of the breakdown site within the STI opening area ($\approx 0.3\ \mu m^2$). For example, if the breakdown happens near the interface of the n well and the STI, a current leakage path may form. This is likely the situation of LED1 with the lowest SMF-coupled power since it also has the lowest forward bias.

In Fig. S6, we plot the performance of LED2, which has intermediate SMF-coupled power in Fig. S5 (a), after on/off switch for $\approx 10^5$ times as a robustness test. After the test, the SMF-coupled power dropped by approximately 25%. As we mentioned in the main text, this is probably due to the lateral propagation of the breakdown site which also leads to the forward bias lowering.

In the main text, we mainly present the device performance of LED2 after the robustness test.

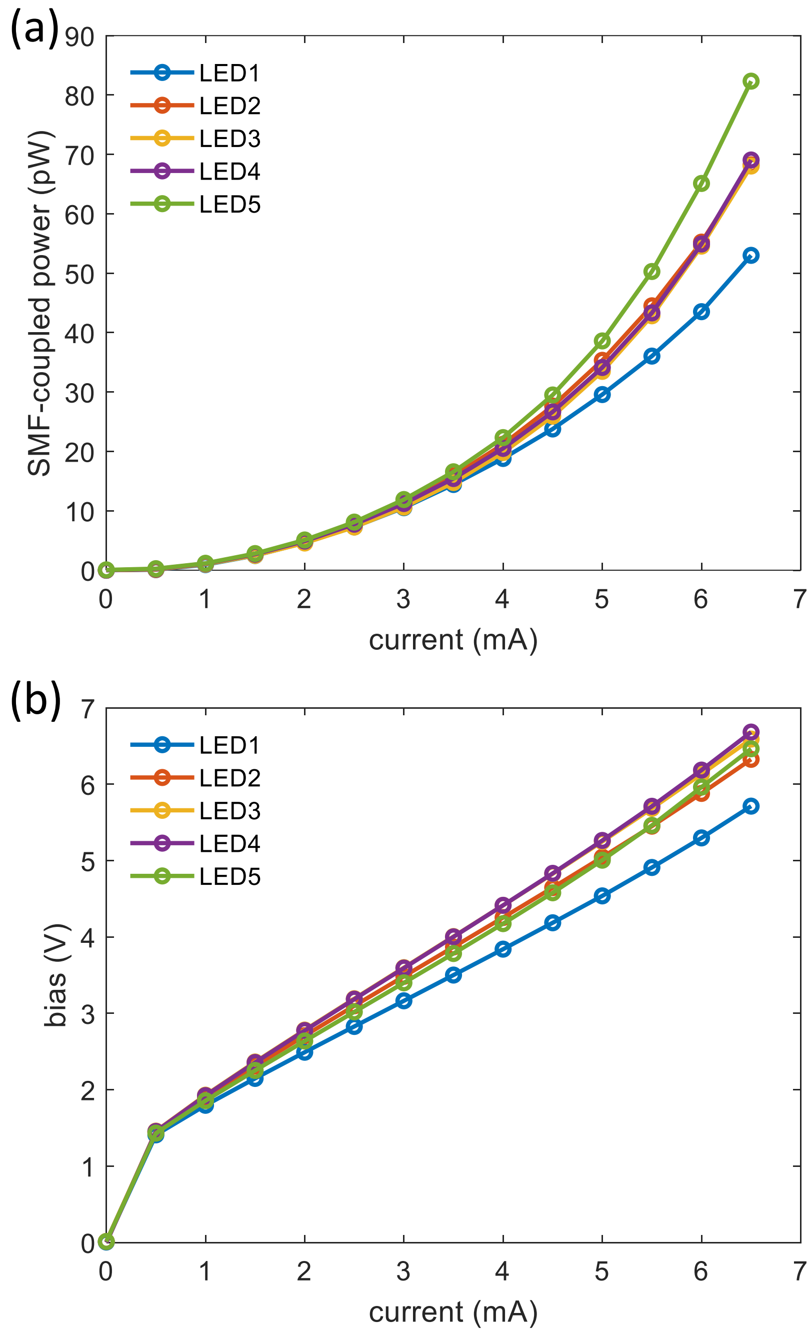

Figure S5. (a) Single mode fiber (SMF) coupled power and (b) bias versus current in five LEDs on different chip dies after gate oxide breakdown.

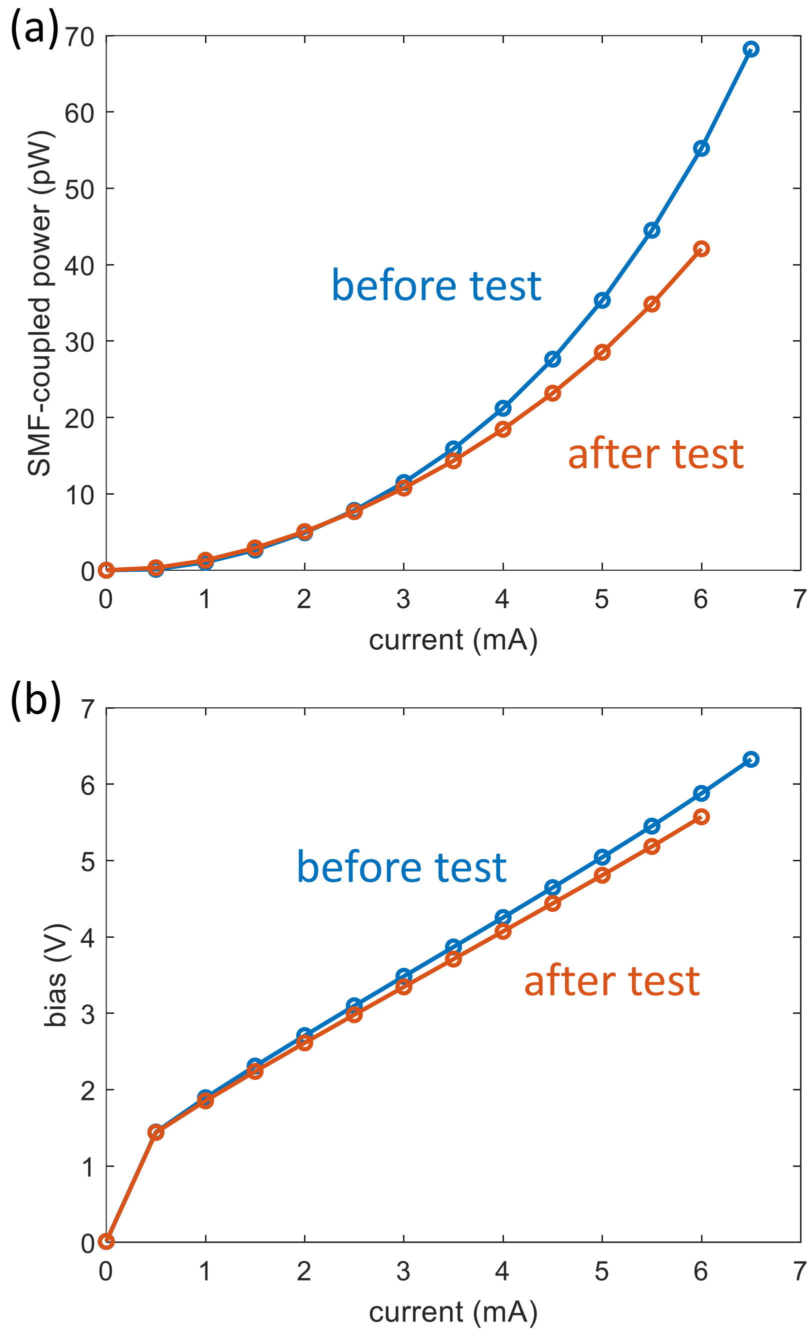

Figure. S6. SMF-coupled power and bias versus current in a LED before and after $\approx 10^5$ on/off switch.

S7. Reference emitter

The characterization results of the reference emitter are presented in Fig. S7. Fig. S7 (a) is a micrograph of the reference emitter biased at 0.9 mA taken by our microscope. Fig. S7 (b) shows the emission pattern. The emission can be fit into a 2D Gaussian function of which the FWHMs are approximately 1 μm.

Fig. S7 (c) shows the emission spectra at various currents. As discussed in the main text, compared with the LED, the reference emitter has a much broader emission spectrum, which indicates that the emission is mainly from impact ionization and hot carrier transition.

Fig. S7 (d) shows the SMF-coupled power and the bias versus the current in the reference emitter. The IV curve of the reference emitter is approximately linear and the resistance is approximately $20k\Omega$. The SMF-coupled power of the reference emitter has a current threshold, which corresponds to the bias when the hot holes have high enough kinetic energy to introduce impact ionization. Compared with Fig. S5, we conclude that the reference emitter has a distinct transport mechanism different from the LED.

Although most of the reference emitters could be biased up to approximately 1 mA, we noticed that the emission power started to degrade when the current was around 0.9 mA. Similar to the LEDs, this is likely due to lateral propagation of the breakdown site.

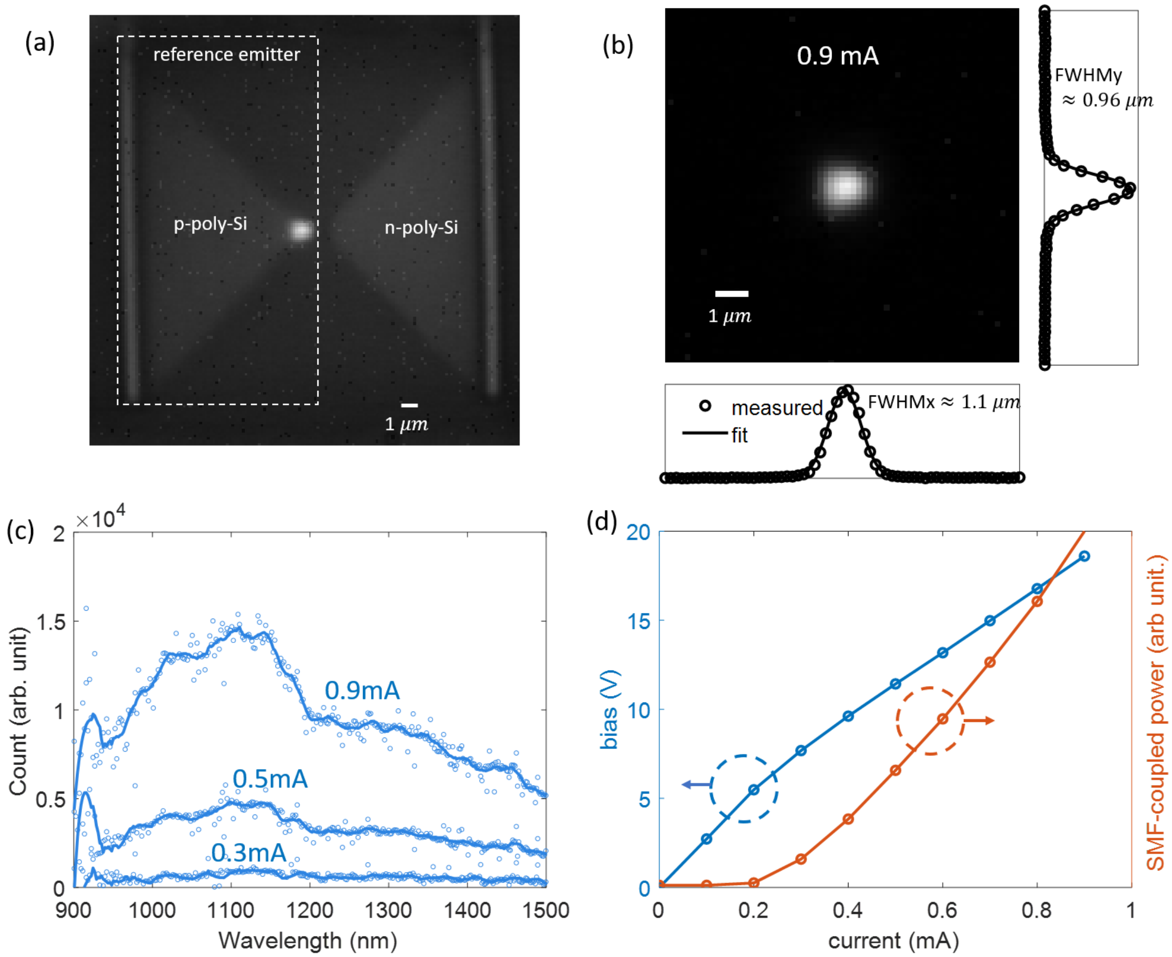

Figure. S7. Characterization of the reference emitter. (a) micrograph; (b) emission pattern; (c) emission spectrum; (d) SMF-coupled power and bias versus current.